European Cells and Materials Vol.56 2026 (pages 22–33) DOI: 10.22203/eCM.v056a02 ISSN 1473-2262

Original Article

PBVHx NANOPARTICLE-MEDIATED GINSENOSIDE Rg3 NANOCARRIERS ENHANCE OSTEOGENIC DIFFERENTIATION OF STEM CELLS

Chengjian Cao[1,§], Fang Zhang[1,§], Juan Tang[1], Dechao Yuan[2], Fuqiang Shao[3], Chenyuan Wang[3], Shiwei Liu[2,*] and Daixu Wei[1,*]

[1]Zigong Academy of Medical Sciences, Zigong First People's Hospital, 643000 Zigong, Sichuan, China
[2]Department of Orthopedics, Zigong First People's Hospital, 643000 Zigong, Sichuan, China
[3]Department of Nuclear Medicine, Zigong First People's Hospital, 643000 Zigong, Sichuan, China
[§]These authors contributed equally.

Abstract

Background: Osteoporosis, a metabolic disorder with reduced bone density and high fracture risk, can be alleviated by ginsenoside Rg3 (GRg3), which promotes human bone marrow-derived mesenchymal stem cell (hBMSC) osteogenic differentiation via multiple pathways. However, GRg3's clinical use is limited by hydrophobicity, short half-life, and degradation susceptibility. **Methods:** This study developed a novel nanocarrier using biodegradable poly (3-hydroxybutyrate-co-3-hydroxyvalerate-co-3-hydroxyhexanoate) (PBVHx) (the latest terpolymer in polyhydroxyalkanoates) doped with a small amount of poly (lactic-co-glycolic acid)-polyethylenimine conjugate (PLGA-PEI) to encapsulate GRg3 (GRg3-PBVHx-based nanoparticles (PNPs)). GRg3-PNPs (1 %, 5 %, 10 % loadings) were spherical, with sizes 105–160 nm (increasing with GRg3) and stable dispersibility. **Results:** Encapsulation efficiency was ~ 89 % for 1 % and 5 % groups, but 38.21 % for 10 % due to leakage. *In vitro*, GRg3 released sustainably over 20 days, synchronized with degradation. Cellular experiments showed efficient uptake by hBMSCs. 5 % and 10 % GRg3-PNPs enhanced cell viability; the 5 % group exhibited the strongest osteogenic efficacy, with increased alkaline phosphatase (ALP) activity, calcium deposition, upregulated pro-osteogenic markers (collagen type I (*COL-1*), osteocalcin (*OCN*), osteopontin (*OPN*), runt-related transcription factor 2 (*RUNX2*)), and downregulated inhibitory markers (matrix Gla protein (*MGP*), osteoprotegerin (*OPG*)). **Conclusions:** This nanosystem, with 5 % GRg3-PNPs as the optimal formulation, efficiently delivers poorly soluble GRg3 and shows promise for traditional Chinese medicine (TCM)-based osteoporosis treatment and bone regeneration.

Keywords: Polyhydroxyalkanoates, ginsenoside, osteoporosis, nanocarriers, stem cells.

***Address for correspondence**: Daixu Wei, Zigong Academy of Medical Sciences, Zigong First People's Hospital, 643000 Zigong, Sichuan, China. Email: daviddxwei@163.com; Shiwei Liu, Department of Orthopedics, Zigong First People's Hospital, 643000 Zigong, Sichuan, China. Email: lsw8896179@163.com.

Introduction

Osteoporosis is a metabolic condition marked by diminished bone mineral density and breakdown of the bone's microstructural framework, which results in heightened bone brittleness and a greater likelihood of fractures. Metabolomic studies and clinical practice have identified certain traditional Chinese medicine (TCM) components that can prevent or treat osteoporosis by promoting proliferative growth, enhancing specialized cell development, and regulating bone metabolism [1]. Ginsenoside Rg3 (GRg3), an active compound extracted from Panax ginseng, exhibits multifaceted regulatory effects on osteoinduction. By modulating key signaling pathways, GRg3 regulates the balance between bone formation and resorption, offering a novel therapeutic perspective for bone metabolic diseases like osteoporosis.

GRg3 triggers the transforming growth factor-beta 1 (TGF-β1)/Smad signaling pathway, stimulating the proliferation and differentiation of osteoblasts and consequently boosting bone formation [2]. GRg3 can also significantly enhance the activity of the Adenosine 5'-monophosphate-activated protein kinase (AMPK) signaling pathway, promote autophagy, osteogenic differentiation and mineralization, and inhibit the mTOR signaling pathway [3]. Regarding the suppression of bone resorption, GRg3 in-

hibits osteoclast differentiation and reduces bone destruction through the receptor activator of nuclear factor-kappa b ligand (RANKL), c-Jun N-terminal kinase (JNK) and p38 mitogen-activated protein kinase (MAPK) pathways [4]. GRg3 modulates the karyopherin alpha 2 (KPNA2) and nuclear factor-kappa b (NF-κB) signaling pathways to influence bone homeostasis, thereby alleviating osteoporosis [5]. Additionally, Rg3 inhibited cytokines and increased the content of antioxidant enzymes to reduce pulmonary inflammation and neutrophil infiltration [6,7]. It can also promote mitochondrial biogenesis and respiration, all of which are indirectly associated with the osteogenic differentiation of stem cells [8].

Unlike the hydrophilic ginsenosides Rg1 and Rg2, GRg3 is a hydrophobic small molecule, which restricts its effectiveness in promoting stem cell proliferation and osteogenic differentiation in both *in vitro* and *in vivo* models. Nanotechnology and biomaterials can enhance the dispersibility of drugs and precisely control their *in vitro* and *in vivo* delivery [9]. To overcome these limitations of GRg3, various nanoparticles and drug carriers have been employed for its loading and release, drawing on advanced drug delivery systems and nanoscale carriers [10–12]. Zhang *et al*. [13] utilized methoxy poly(ethylene glycol) succinic acid (mPEG-SA) with bovine serum albumin (BSA) as a nanocarrierto improve the hydrophobicity of GRg3, demonstrating superior anticancer efficacy compared to free Rg3. However, the encapsulation efficiency (EE) of GRg3 was only 76.56 %, still resulting in significant drug wastage. Therefore, a novel drug loading (DL) and release system is needed to further advance the clinical application of the TCM component GRg3 in osteoporosis treatment.

In previous studies, we utilized the hydrophobic material poly(3-hydroxybutyrate-co-3-hydroxyvalerate-co-3-hydroxyhexanoate) (PBVHx) to encapsulate hydrophobic small-molecule drugs within nano-sized particles or microspheres, enabling sustained release [14,15]. PBVHx nanoparticles effectively reduce drug toxicity while ensuring slow release [14]. Furthermore, we found that adding a small amount of poly(lactic-co-glycolic acid)-polyethylenimine conjugate (PLGA-PEI) during PBVHx nanoparticle preparation significantly enhances cellular uptake [16,17]. PBVHx is a novel terpolymer member of the microbially synthesized polyhydroxyalkanoate (PHA) family. Owing to its more complex monomer composition (including 3-hydroxybutyrate (3HB), 3-hydroxyvalerate (3HV), and 3-hydroxyhexanoate (3HHx)), the material exhibits degradation kinetics that are more manageable. This advantage also makes it more suitable to act as a long-term delivery system for components extracted from TCM. In comparison to polylactic acid (PLA) and PLGA, PBVHx is a type of biopolyester that degrades at a slower pace and has more excellent biocompatibility [18–21].

We propose applying a PBVHx-based composite nanosystem doped with a small amount of PLGA-PEI for GRg3 delivery. This approach aims to enrich the research on delivery carriers for TCM active ingredients, explore the regulatory mechanisms of biocompatible polymers on the dispersibility of hydrophobic drugs, and provide a reference for optimizing the formulation of other small-molecule TCM components.

Materials and Methods

Materials

Medical grade poly(3-hydroxybutyrate-co-3-hydroxyvalerate-co-3-hydroxyhexanoate) (PBVHx, molecular weight = 46 kDa, composition: 90 mol % 3-hydroxybutyrate (3HB), 3 mol % 3HV, 7 mol % 3HHx) was obtained from BluePHA (Beijing Bluepha Microbiology Technology Co., Ltd., Beijing, China). Poly(lactic-co-glycolic acid)-polyethylenimine conjugate (PLGA-PEI) was synthesized from Daigang (Jinan Daigang Biotechnology, 2810, Jinan, China). Polyvinyl alcohol (PVA, 94.5 % hydrolyzed) was obtained from Sigma-Aldrich (Sigma-Aldrich, 341584, St. Louis, MO, USA). Ginsenoside Rg3 (GRg3) was purchased from Aladdin (Aladdin, G107681, Shanghai, China).

Preparation of PBVHx-Based Nanoparticles (PNPs)

GRg3-loaded PNPs (GRg3-PNPs) were prepared using a modified emulsion-solvent evaporation method, as detailed in Table 1 and previously described [14,19]. Briefly, 1 mg, 5 mg, or 10 mg of GRg3, 1 g PBVHx, and 1 mg PLGA-PEI were dissolved in 20 mL of a mixed organic solvent consisting of dichloromethane (Aladdin, D116144, Shanghai, China) and dimethyl sulfoxide (DMSO; 99.5:0.5, v/v, Aladdin, D670381, Shanghai, China). To form the aqueous phase, 1 g of PVA was dissolved in 100 mL of distilled water, and this dissolution was done at a temperature of 80 °C. The two phases were effectively separated through ultrasonic treatment lasting 1 minute in an ice-water bath. The removal of dichloromethane was achieved by evaporating it at 30 °C, a process that took 30 minutes. Next, to eliminate any remaining PVA, centrifugation was conducted at 12,000 rpm over a 10-minute period. Control groups included pure PNPs (pPNPs) without GRg3. To track cellular uptake, coumarin 6 (C6, 0.01 mg, Aladdin, C100929, Shanghai, China), a green fluorescent dye, was dissolved in 5 mL dichloromethane and incorporated into some PNPs during preparation.

Characterization of PNPs

A Zetasizer Nano-ZS90 (Malvern Panalytical, Malvern, Worcestershire, UK) was used to determine the size distribution of all nanoparticles, with measurements taken at 25 °C. Scanning electron microscopy (SEM, Hitachi S-4800, Tokyo, Japan) and transmission electron microscopy (TEM, JEOL JEM-1200EX, Tokyo, Japan) were employed to examine the morphological features of

Table 1. Composition comparison of various PNPs in this study.

PNPs	PBVHx/mg	PLGA-PEI/mg	GRg3/mg	DCM/mL	DMSO/mL
pPNPs	1000.0	1.0	0	19.9	0.1
1 % GRg3-PNPs	1000.0	1.0	1.0	19.9	0.1
5 % GRg3-PNPs	1000.0	1.0	5.0	19.9	0.1
10 % GRg3-PNPs	1000.0	1.0	10.0	19.9	0.1

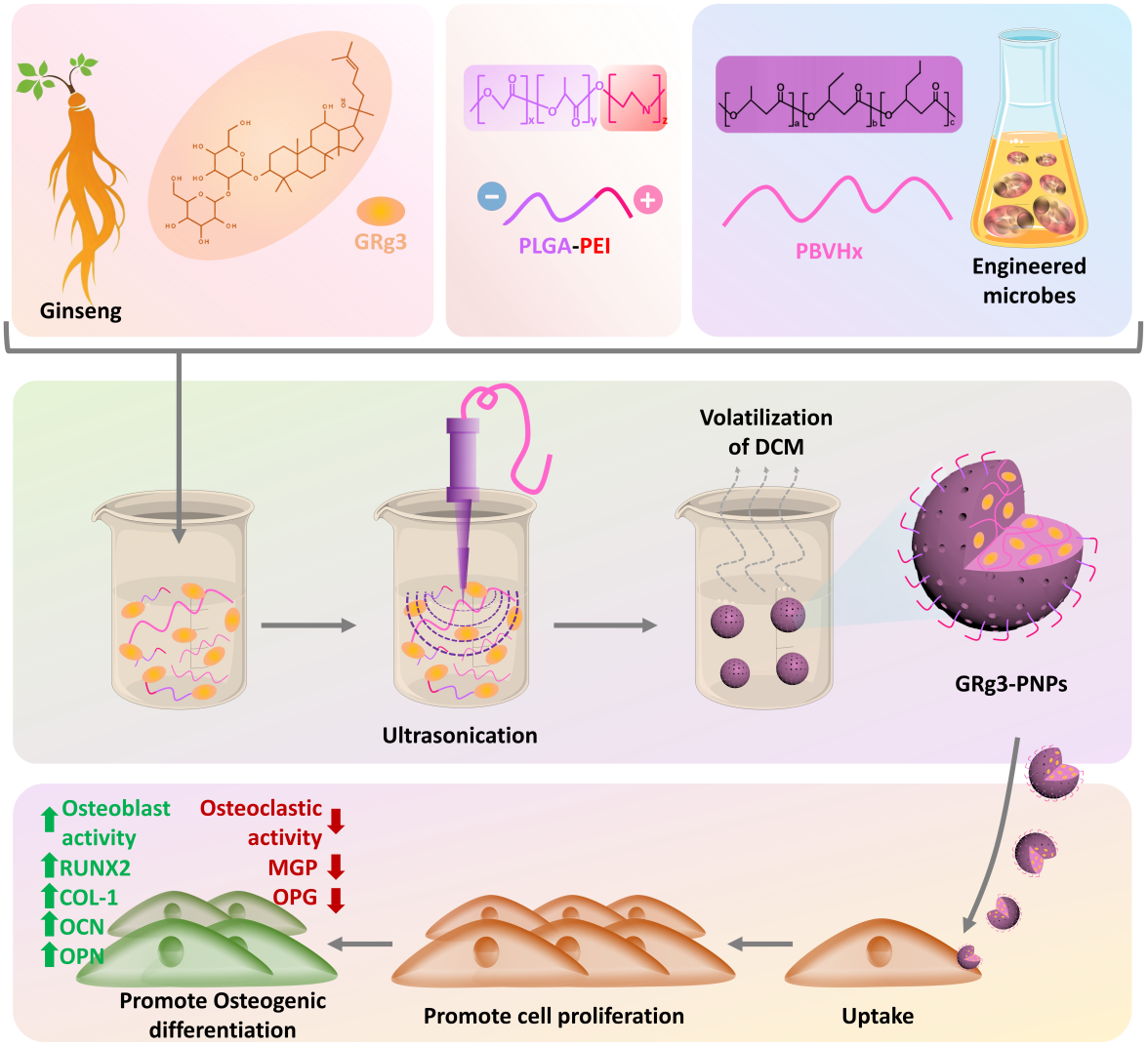

Fig. 1. Schematic of the GRg3-loaded PBVHx-based hybrid nanoparticles (GRg3-PNPs) in this study, including the composition, preparation, and osteogenic induction tests of GRg3-PNPs. This figure was created using PowerPoint.

all nanoparticles (PNPs).

Encapsulation Efficiency and Drug Loading of GRg3

The encapsulation efficiency (EE) and drug loading (DL) of GRg3 within GRg3-PNPs were assessed using a previously reported method [17]. The total amount of GRg3 used (W_0) and the amount of unencapsulated free GRg3 dissolved in the supernatant (W_1) were determined using high-performance liquid chromatography (HPLC).

EE was calculated using Equation (1): EE (%) = ((W_0 – W_1) / W_0) × 100 %

DL was calculated using Equation (2): DL (%) = ((W_0 – W_1) / W_2) × 100 %

Where W_0 is the total amount of GRg3 used in preparation. W_1 is the amount of free GRg3 that was not encapsulated into the PNPs and remained dissolved in the supernatant. W_2 is the mass of the PNPs.

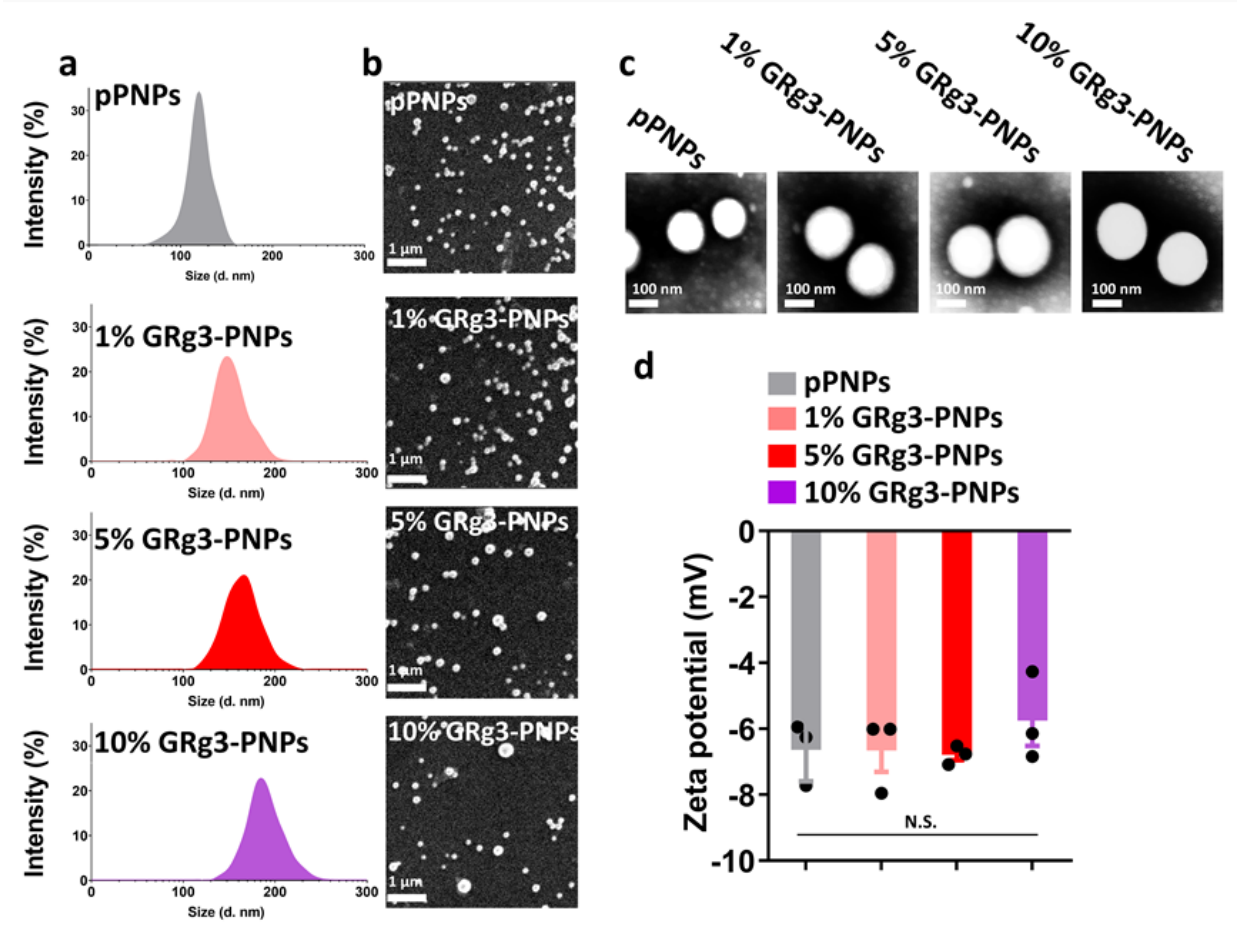

Fig. 2. Characterization of various PNPs. (**a–d**) Size distribution (**a**), SEM images (**b**), TEM images (**c**), and zeta potential (**d**) of pPNPs, 1 % GRg3-PNPs, 5 % GRg3-PNPs, and 10 % GRg3-PNPs, respectively. The scale bars are 1 μm in (**b**) and 100 nm in (**c**). Three parallel measurements for (**d**). N.S. = no significant difference.

In Vitro Release of GRg3 from PNPs and Degradation Behaviors

A dialysis approach was used to analyze how GRg3 is released from PNPs *in vitro*. One milliliter of GRg3-PNPs suspension was put into a dialysis bag (SIGMA, D9652, St. Louis, MO, USA) and then incubated with shaking (50 rpm) at 37 °C. This incubation took place in 8 milliliters of release medium (phosphate-buffered saline (PBS), pH 7.2, Thermo Scientific, J62899, Waltham, MA, USA) for set time periods. At each time point, the release medium that contained GRg3 which had permeated through was collected. It was then replaced with a new medium. The amount of ginsenoside Rg3 released was determined by high-performance liquid chromatography (HPLC), following the method described in the previous report [22].

The residual weight of dried PNPs was calculated using Equation (3): Weight loss (%) = (W_3 / W_4) × 100 %

Where W_3 is the weight of residual PNPs and W_4 is the initial weight of total PNPs. Each sample was measured in triplicate (n = 3).

The cumulative release of GRg3 from PBVHx PNPs was calculated using Equation (4): Cumulative release (%) = (B_1 / B_0) × 100 %

Where B_1 is the cumulative amount of GRg3 released at time t and B_0 is the total amount of GRg3 loaded. Each sample was measured in triplicate (n = 3).

Cell Culture and Viability Assessment

Cultivation of human bone marrow-derived mesenchymal stem cells (hBMSCs, Cyagen Biosciences, HUXMA-01001, Suzhou, China) occurred in Basal Medium (BM, Cyagen Biosciences, BLDM-03011, Suzhou, China). The medium included 10 % fetal bovine serum (FBS, Cyagen Biosciences, FBSSR-01021-500, Suzhou, China) and 1 % penicillin-streptomycin solution (Beyotime, C0222, Shanghai, China). These cells were kept in a moist 5 % Carbon Dioxide (CO_2) atmosphere at 37 °C. For the evaluation of cell viability, 10^5 hBMSCs were seeded into 24-well tissue culture plates (TCP, i-Quip, C7065, Shanghai, China) and incubated for 24 hours. Next, the cells were exposed to 100 μL of pPNPs or GRg3-PNPs, both at 10 μg/mL concentration, for 1, 7, 14,

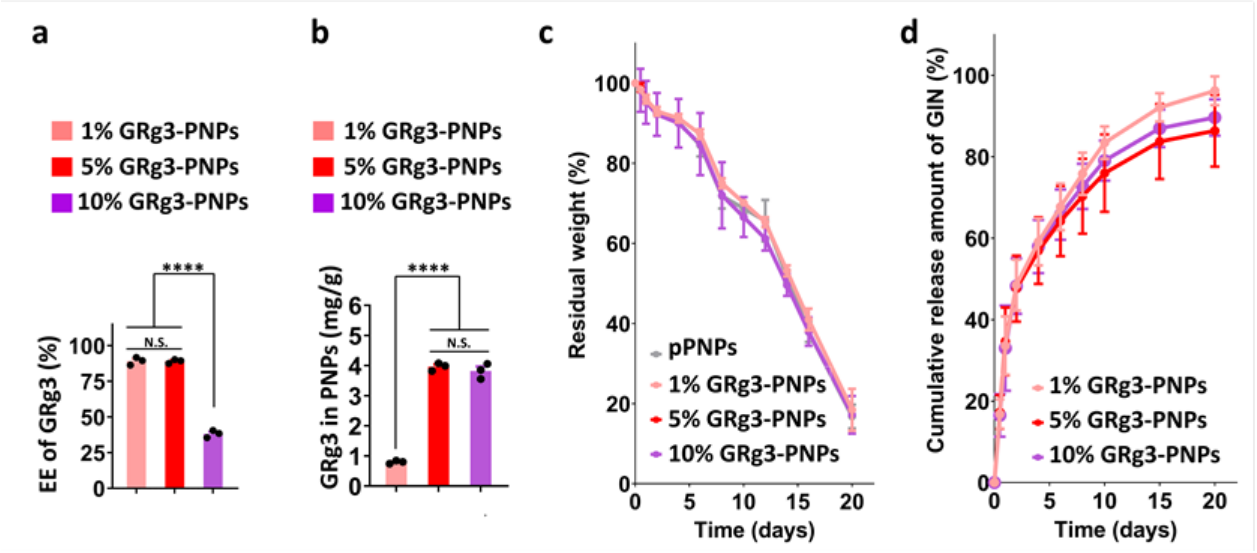

Fig. 3. Loading and release of GRg3 in various PNPs. (**a**) Entrapment efficiency (EE) and (**b**) drug loading (DL) of GRg3 and GRg3 in PNPs for 1% GRg3-PNPs, 5% GRg3-PNPs, and 10% GRg3-PNPs, respectively. (**c**) Residual weight (%) of pPNPs, 1 % GRg3-PNPs, 5 % GRg3-PNPs, and 10 % GRg3-PNPs, respectively, immersed in PBS with 1 mg/mL lipase under constant shaking at 50 rpm and 37 °C (n = 3). (**d**) Cumulative release of GRg3 (%) from 1 % GRg3-PNPs, 5 % GRg3-PNPs, and 10 % GRg3-PNPs, respectively, immersed in PBS with 1 mg/mL lipase under constant shaking at 50 rpm and 37 °C. Three parallel measurements for (**a–d**). N.S. = no significant difference. ****$p < 0.0001$.

and 21 days. After the treatment phase, cell viability was determined with the cell counting kit-8 (CCK-8, Aladdin, C266180, Shanghai, China). Every experimental condition was tested six times (n = 6).

Cellular Uptake of PNPs

A quantity of 10^5 hBMSCs was seeded into 6-well TCPs and allowed to culture for 24 hours. The cells were then treated with 100 μL of C6-labeled pPNPs or GRg3-PNPs for a period of 1 day. Following this, the cells were washed with PBS and fixed using 4 % formaldehyde (Aladdin, C104188, Shanghai, China). Next, actin filaments were stained with Alexa Fluor™ 555 phalloidin (Thermo Fisher Scientific, A34055, USA), while nuclei were stained with 4′,6-diamidino-2-phenylindole (DAPI; Thermo Fisher Scientific, D21490, USA). The cellular uptake and surface binding of the PNPs were observed with the use of a confocal laser scanning microscope (CLSM; Nikon, A1 HD25/A1R HD25, Tokyo, Japan).

Osteogenic Differentiation Staining

The low-concentration osteogenic differentiation medium includes 50 % standard osteogenic differentiation medium (OM, Cyagen Biosciences, HUXMX-90021, Suzhou, China) and 50 % BM, which is used to stimulate the osteogenic differentiation of hBMSCs for 20 days. It contains 5 mM β-glycerophosphate sodium, 0.5 mM ascorbic acid-2-phosphate, and 50 nM dexamethasone. The stained cells were visualized under a microscope (Nikon, Tokyo, Japan). The calcium deposition of cells was stained using the Osteogenesis Assay Kit (Beyotime, C0148S, Shanghai, China) and mean red intensities of each well were measured using Fiji/ImageJ 1.54m software (https://imagej.net/software/fiji/). Additionally, alkaline phosphatase (ALP) activity and calcium deposition were respectively detected using commercial ALP staining (Beyotime, P0321S, Shanghai, China).

Alkaline Phosphatase (ALP) Activity Assay

ALP activity was quantified using a commercial ALP assay kit (Beyotime, P0321M, Shanghai, China). A total of 10^5 hBMSCs were plated in 6-well TCPs and incubated for 24 hours. The cells were then exposed to pPNPs, GRg3-PNPs, or control medium for 21 days, with ALP expression assessed at 1, 7, 14, and 21 days, respectively.

Quantitative Real-Time Polymerase Chain Reaction (qRT-PCR) Analysis

To assess the messenger RNA (mRNA) expression levels of six bone repair-related markers, qRT-PCR was applied. The markers in question include collagen type I (*COL-1*), osteocalcin (*OCN*), osteopontin (*OPN*), runt-related transcription factor 2 (*RUNX2*), matrix Gla protein (*MGP*), and osteoprotegerin (*OPG*). The QuantiTect SYBR Green PCR Kit (Qiagen, 204143, Hilden, Germany) was employed, and glyceraldehyde-3-phosphate dehydrogenase (*GAPDH*) served as the internal reference gene. Triplicate analyses were conducted for each sample.

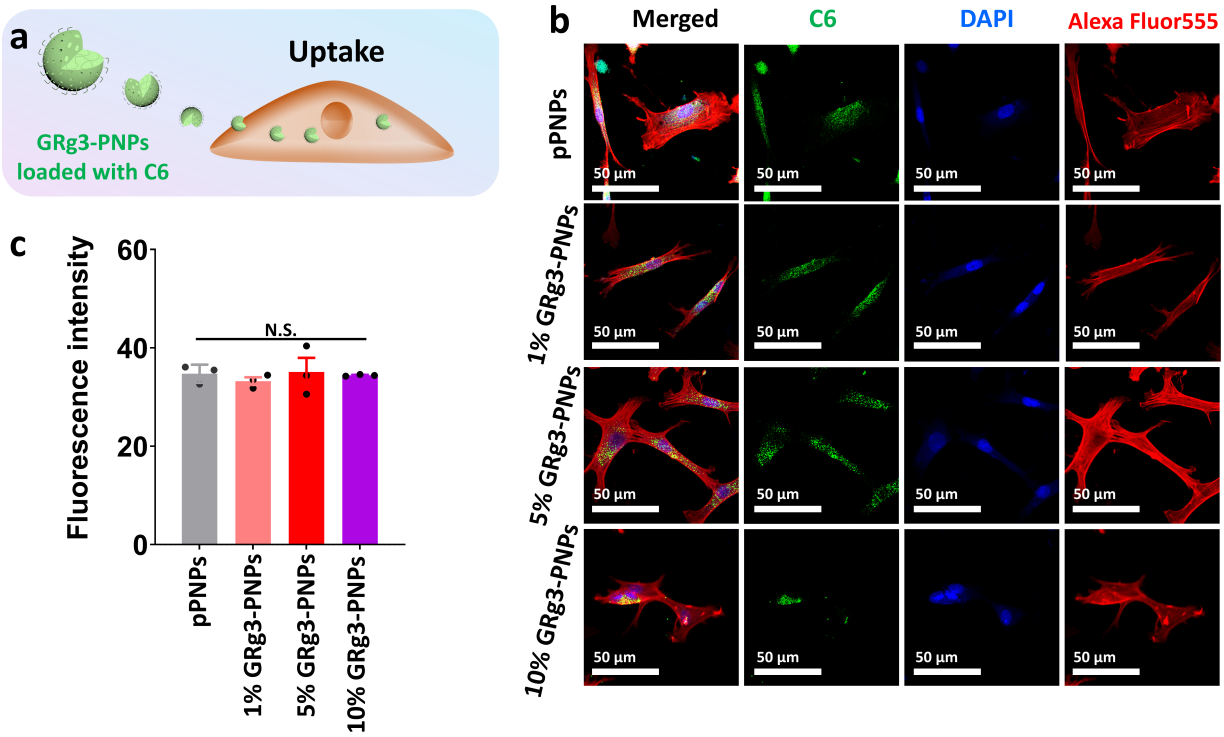

Fig. 4. Uptake and intracellular distribution of various PNPs in hBMSCs. (**a**) Schematic of the uptake of coumarin 6 (C6)-loaded GRg3-PNPs by hBMSCs. (**b**) Confocal laser-scanning microscopy images of hBMSCs treated with pPNPs, 1 % GRg3-PNPs, 5 % GRg3-PNPs, and 10 % GRg3-PNPs, respectively, labeled with green fluorescent C6 for 2 hours. The scale bar is 50 μm. (**c**) Relative green fluorescence intensity of pPNPs, 1 % GRg3-PNPs, 5 % GRg3-PNPs, and 10 % GRg3-PNPs in hBMSCs. n = 3. N.S. = no significant difference.

Statistical Analysis

All experimental data are expressed in the form of mean ± standard deviation (SD). The evaluation of statistical significance was carried out using one-way analysis of variance (ANOVA), and a p-value < 0.05 was defined as statistically significant. All statistical tests were conducted with Prism 5 software (GraphPad Software, San Diego, California, USA).

Results

Properties of GRg3-Loaded PNPs

The primary objective of this study was to develop a nanoparticle-mediated approach to enhance the dispersibility of poorly soluble ginsenoside Rg3 to induce hBMSC transformation. To this end, we designed a nanoscale controlled-release system based on the biopolyester PBVHx, as illustrated in Fig. 1.

As shown in Fig. 2**a**, the peak particle size distribution of blank control pPNPs (without GRg3) was approximately 105 nm. The sizes of GRg3-loaded PNPs increased with GRg3 content: 1 % GRg3-PNPs (~ 120 nm), 5 % GRg3-PNPs (~ 135 nm), and 10 % GRg3-PNPs (~ 160 nm). SEM and TEM analyses (Fig. 2**b**,**c**) revealed similar spherical morphology and uniform distribution for both pPNPs and GRg3-PNPs, although differences in particle size were evident.

The surface charge (zeta potential) of all nanoparticles ranged between –4 mV and –8 mV (Fig. 2**d**). These results indicate that incorporating GRg3 into PBVHx/PLGA-PEI nanoparticles did not significantly affect their dispersibility, uniformity, or surface characteristics. However, the particle size of GRg3-PNPs increased progressively with higher GRg3 concentrations.

As shown in Fig. 3**a**, at low GRg3 concentrations, the EE of GRg3 in 1 % GRg3-PNPs (89.22 %) and 5 % GRg3-PNPs (89.08 %) was similar and notably higher than the previously reported 76.56 % for other GRg3 nanocarriers [13]. However, when the theoretical GRg3 concentration reached 10 %, the EE for 10 % GRg3-PNPs dropped significantly to only 38.21 %. Conversely, the DL per gram of nanoparticles was 0.80 mg for 1 % GRg3-PNPs, 3.40 mg/g for 5 % GRg3-PNPs, and 3.82 mg/g for 10 % GRg3-PNPs (Fig. 3**b**). These findings suggest that excess GRg3 cannot be fully encapsulated, leading to leakage of free drug and reduced EE, while insufficient GRg3 concentration fails to saturate the loading capacity of the PNPs.

Release of GRg3 from GRg3-PNPs and Degradation

The *in vitro* release profile of GRg3 from pPNPs and GRg3-PNPs over 20 days in degradation medium was studied using dynamic dialysis. Throughout the 20-day degra-

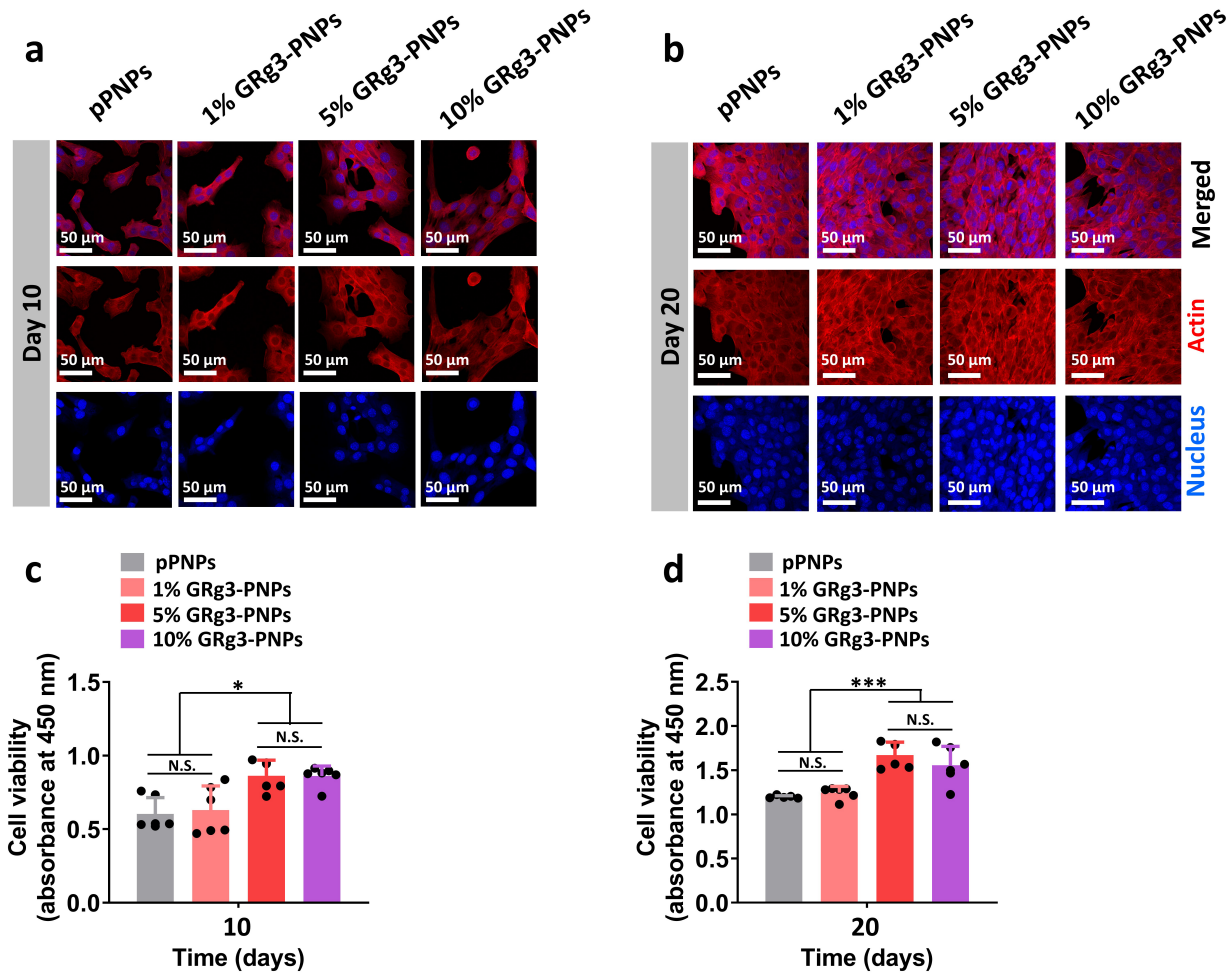

Fig. 5. Cytotoxicity evaluation of various PNPs. (**a,b**) CLSM images of hBMSCs treated with various PNPs for 5 days (**a**) and 10 days (**b**). The scale bar is 50 μm in (**a**) and (**b**). (**c,d**) Cell viability of hBMSCs treated with various PNPs using the CCK-8 assay for 5 days (**c**) and 10 days (**d**). n = 6. N.S. = no significant difference; *$p < 0.05$; ***$p < 0.001$.

dation period, all three GRg3-PNPs exhibited similar degradation behavior. The residual weight percentages of PNPs were 86.74 %–93.51 % on day 4, 65.80 %–70.05 % on day 10, and 13.22 %–19.63 % on day 20 (Fig. 3**c**). This indicates that the presence of GRg3 did not significantly interfere with PNPs degradation. As shown in Fig. 3**d**, GRg3-PNPs exhibited a burst release of 15.08 %–19.02 % GRg3 within the initial 0.5 days, which was subsequently followed by a prolonged sustained-release phase. By day 20, GRg3 was almost completely released from all GRg3-PNPs (82.42 %–97.26 %), with no significant differences observed between groups ($p > 0.05$). The trend of GRg3 release closely paralleled the degradation behavior of the PNPs, further confirming that GRg3 does not significantly interfere with nanoparticle degradation or drug release kinetics. The size distribution of the four types of nanoparticles before and after degradation was characterized using a particle size analyzer. It is evident that the size distribution of all nanoparticles shifted to the left on Day 20 of degradation (**Supplementary Fig. 1**), which further confirms the degradation behavior of PBVHx.

Intracellular and Surface Distribution of PNPs in hBMSCs

To directly visualize nanoparticle distribution, hBMSCs were incubated with green fluorescent coumarin 6 (C6)-labeled pPNPs and GRg3-PNPs for 2 hours (schematic in Fig. 4**a**). As expected, green fluorescent C6-PNPs were predominantly internalized by hBMSCs under all conditions (Fig. 4**b**). Fluorescence intensity analysis showed no significant differences between the four types of PNPs ($p > 0.05$) (Fig. 4**c**). These results demonstrate that the amount of PNPs taken up by cells or bound to the cell surface was equivalent, implying that GRg3 did not affect the cellular uptake capability of the PNPs.

Biocompatibility of Cells Incubated with PNPs

As shown in Fig. 5**a,b**, hBMSCs treated with pPNPs, 1 % GRg3-PNPs, 5 % GRg3-PNPs, and 10 % GRg3-PNPs exhibited normal proliferation over 20 days, as confirmed by CLSM observation after phalloidin (red) and DAPI (blue) staining. The results of the CCK-8 assay (Fig. 5**c**) showed that on day 10, the cell viability in the pPNPs

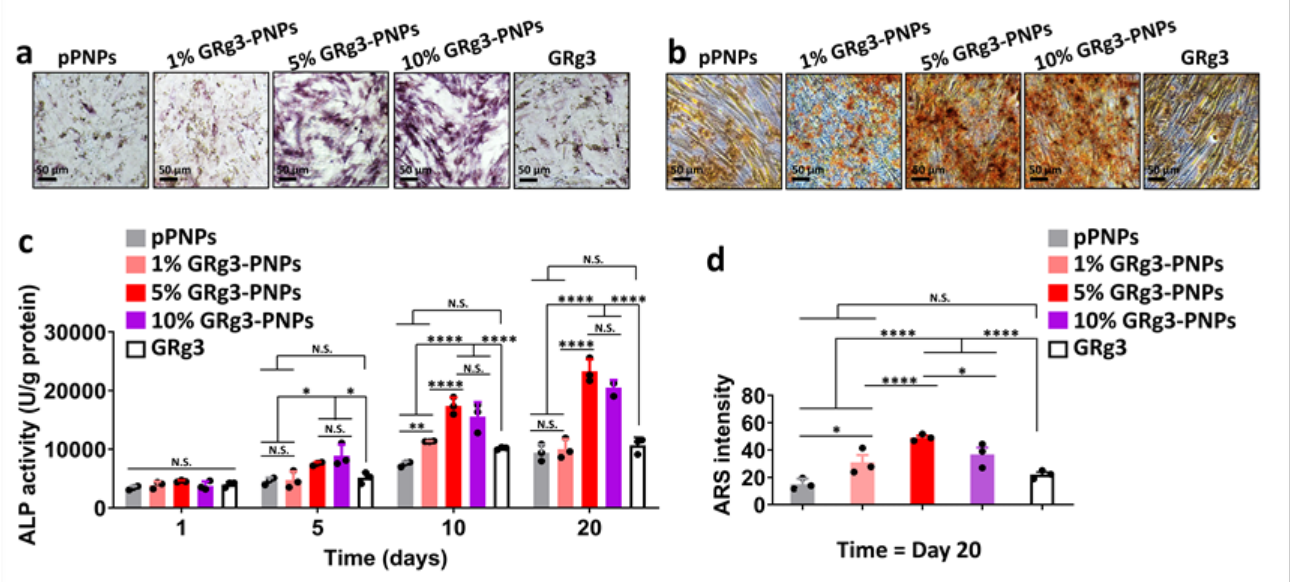

Fig. 6. Osteogenic effect of various PNPs and GRg3 alone. (**a**) ALP staining of hBMSCs treated with various PNPs and GRg3 alone for 20 days. (**b**) Alizarin red S (ARS) staining of hBMSCs treated with various PNPs and GRg3 alone for 20 days. (**c**) ALP activity of hBMSCs treated with various PNPs and GRg3 alone for 1, 5, 10, and 20 days (n = 3). (**d**) ARS intensity of hBMSCs treated with various PNPs and GRg3 alone for 1, 5, 10, and 20 days (n = 3). N.S. = no significant difference; *$p < 0.05$; **$p < 0.01$; ****$p < 0.0001$. The scale bar is 50 μm in (**a**) and (**b**).

and 1 % GRg3-PNPs treatment groups was significantly lower compared to the 5 % GRg3-PNPs and 10 % GRg3-PNPs groups (*$p < 0.05$), while there was no statistically significant difference between the 5 % GRg3-PNPs and 10 % GRg3-PNPs groups ($p > 0.05$). By day 20, the cell viability in the 5 % GRg3-PNPs and 10 % GRg3-PNPs groups remained significantly higher than that in the 1 % GRg3-PNPs and pPNPs groups (***$p < 0.001$) (Fig. 5**d**). This suggests that the proliferation phase of hBMSCs was not adversely affected by the nanoparticles and further confirms that GRg3 likely promotes stem cell growth, consistent with previous reports.

Osteogenic Differentiation of hBMSCs by Sustained Intracellular Release of GRg3

After 24 hours of incubation with PNPs to allow uptake, hBMSCs were cultured for an additional 20 days under osteogenic differentiation conditions. Following sustained treatment with GRg3-PNPs containing different amounts of GRg3, assessment of ALP activity and calcium nodule formation revealed that 5 % GRg3-PNPs exhibited the most potent osteogenic effect.

As shown in Fig. 6**a,c**, ALP activity showed no significant differences among the four PNPs groups on day 1. From day 5 onwards, ALP levels in the 5 % GRg3-PNPs and 10 % GRg3-PNPs groups were consistently higher than those in the 1 % GRg3-PNPs and pPNPs groups (*$p < 0.05$ or ***$p < 0.001$). By day 20, ALP activity in the 5 % and 10 % GRg3-PNPs groups was more than double that of the other two groups. On day 20, the level of calcium nodule formation (mineralization) was significantly higher in the 5 % GRg3-PNPs group compared to the 10 % GRg3-PNPs group (*$p < 0.05$), and markedly higher than both the 1 % GRg3-PNPs and pPNPs groups (****$p < 0.0001$) (Fig. 6**b,d**). Due to the poor solubility of GRg3 in water or PBS buffer, directly administered GRg3 failed to effectively stimulate the osteogenic differentiation of BMSCs, resulting in low expression levels of ALP and reduced mineralization (Fig. 6).

Further evaluation using quantitative PCR (qPCR) assessed the mRNA expression of six osteogenic differentiation markers: collagen type I (*COL-1*), osteocalcin (*OCN*), osteopontin (*OPN*), runt-related transcription factor 2 (*RUNX2*), matrix Gla protein (*MGP*), and osteoprotegerin (*OPG*). As shown in Fig. 7**a–d**, the mRNA expression levels of pro-osteogenic markers *COL-1*, *OCN*, *OPN*, and *RUNX2* were significantly upregulated in the 5 % GRg3-PNPs and 10 % GRg3-PNPs groups compared to the 1 % GRg3-PNPs and pPNPs groups (***$p < 0.001$ or ****$p < 0.0001$). Notably, OPN expression was highest in the 5 % GRg3-PNPs group (Fig. 7**c**). Conversely, the mRNA expression levels of *MGP* and *OPG*, markers associated with osteogenesis inhibition or osteoclastogenesis promotion, showed a downregulation trend in the 5 % and 10 % GRg3-PNPs groups (Fig. 7**e,f**). Collectively, these results confirm the potent *in vitro* osteogenic efficacy of both 5 % and 10 % GRg3-PNPs, with 5 % GRg3-PNPs demonstrating optimal performance.

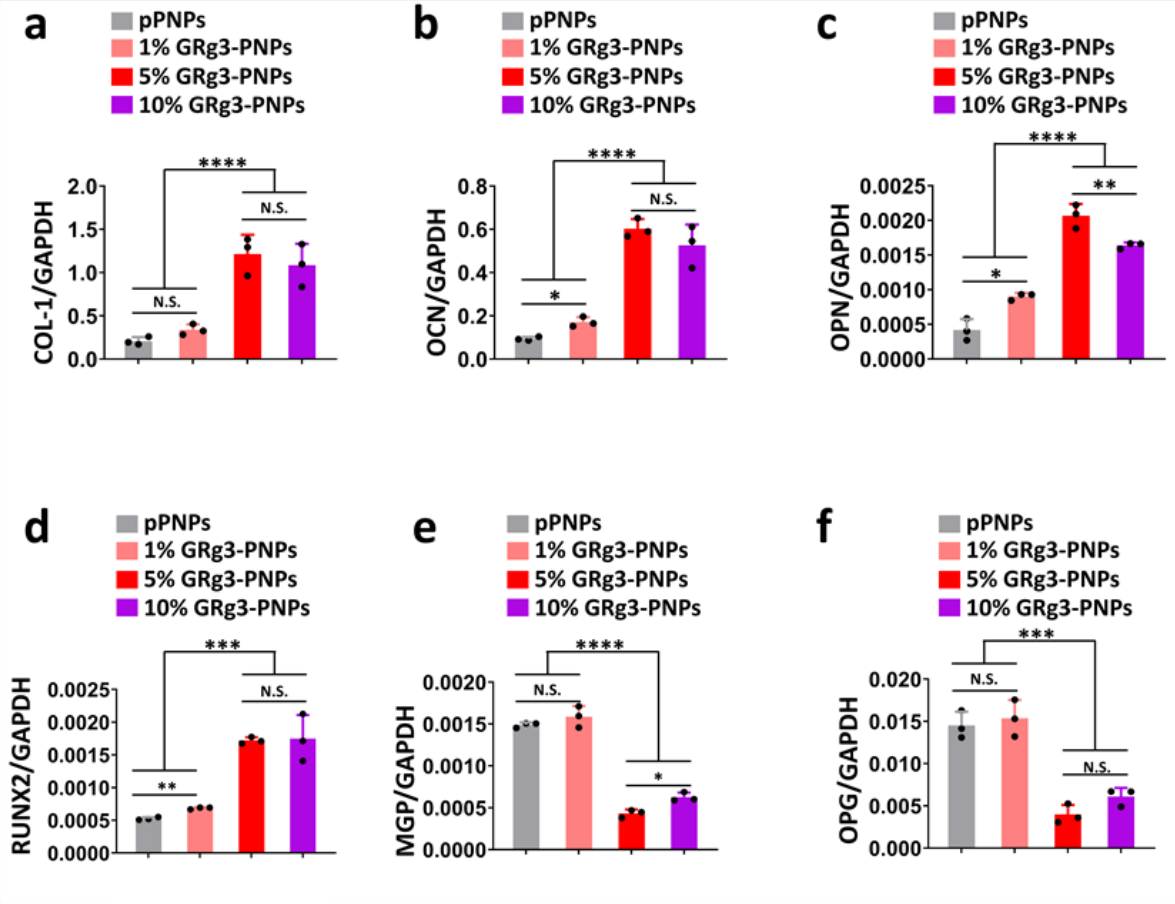

Fig. 7. Quantitative PCR analysis of the mRNA expression of osteogenic biomarkers. (**a**) COL-1, (**b**) OCN, (**c**) OPN, (**d**) RUNX2, (**e**) MGP, and (**f**) OPG, respectively. The y-axis represents the relative expression calculated using the $\Delta\Delta Ct$ method and normalized to GAPDH as the housekeeping gene. n = 3; N.S. = no significant difference; *$p < 0.05$; **$p < 0.01$; ***$p < 0.001$; ****$p < 0.0001$.

Discussion

The poor dispersibility of ginsenosides due to their unique chemical structures leads to low bioavailability, which has consistently limited their clinical application. This issue can be effectively addressed by intelligent drug delivery systems based on various nanocarriers [23,24]. The objective of this study was to develop a nanoparticle-mediated approach based on the novel biodegradable natural polyester PBVHx [20,25] to enhance the dispersibility of poorly soluble ginsenoside Rg3 (GRg3), thereby promoting hBMSC transformation (Fig. 1).

A newer addition to the microbially produced polyhydroxyalkanoate (PHA) family is PBVHx, also referred to as PHBVHHx. The PHA family itself is composed of 3-hydroxybutyrate (3HB), 3-hydroxyvalerate (3HV), and 3-hydroxyhexanoate (3HHx) [26]. With its biocompatible and biodegradable properties, PBVHx is comparable to other PHAs in that it can be turned into microspheres and nanoparticles. These forms of PBVHx find practical use in tissue repair, drug delivery, and the development of vaccines [26]. Furthermore, when PBVHx breaks down, it releases non-toxic monomeric substances, and the main component of these substances is 3-hydroxybutyrate (3HB or BHB) [18,20]. Therefore, in contrast to biodegradable polymers like PLA and PLGA that release lactic acid rapidly, PBVHx stands out as a promising biopolyester for drug delivery applications [15,16].

The incorporation of GRg3 moderately increased nanoparticle size (Fig. 2**a–c**), aligning with our previous findings that increased drug loading leads to larger nanoparticle dimensions [16,17]. This size increase may result from GRg3 molecule aggregation within or on the surface of the PNPs. Owing to the strong lipophilicity of GRg3, it can be dispersed in PBVHx within organic solvents. However, GRg3 did not cause significant aggregation or charge alteration of PNPs compared with pPNPs, indicating that all nanoparticles possessed favorable dispersibility.

Similar to PLA, PNPs are a type of carrier with a strong negative charge ranging from –42 mV to –38 mV [17]. In contrast to other positively charged materials (e.g., chitosan), this strong negative charge is unfavorable for the contact between PNPs and cells that also carry negative surface charge, which further results in a decline in cellular uptake capacity. Therefore, in our previous studies,

poly-L-lysine and PLGA-PEI were utilized, respectively, to neutralize the majority of charges on the surface of PNPs [16,17]. This treatment attenuated the surface charge to a range of –4 mV to –8 mV (Fig. 2**d**). Given the low content of PLGA-PEI, its inherent positive charge was sufficient to neutralize most of the negative charge on the surface of PNPs, thus converting the strong negative charge of pristine PNPs into weak negative charge, which ultimately enhanced the cellular uptake of the nanoparticles.

Therefore, cellular uptake assays demonstrated that the green fluorescent PNPs were predominantly internalized by hBMSCs, with comparable fluorescence intensities observed across all groups. This indicates that GRg3 loading did not compromise the cellular uptake capability of the PNPs (Fig. 4**b,c**). However, the pure PNPs exhibit weaker cellular uptake compared to PBVHx/PLGA-PEI composite nanoparticles (PNPs) in previous study [17], primarily due to PEI enhancing the overall surface charge of the nanoparticles.

To explore the maximum loading capacity of GRg3, PNPs with theoretical GRg3 loadings of 1 %, 5 %, and 10 % were evaluated for EE and DL. The results clearly show that excess GRg3 cannot be fully encapsulated, leading to drug leakage and wastage (low EE for 10 % loading). However, within a certain range, increasing the theoretical GRg3 concentration enhances the DL capacity of the PNPs (Fig. 3**a,b**). Therefore, selecting an appropriate GRg3 concentration is paramount to achieving an optimal balance between EE and DL. Based on this, 5 % GRg3-PNPs represent the best compromise between high EE and substantial DL, while 10 % GRg3-PNPs also possess strong GRg3 loading capacity; both were consequently selected for further investigation.

During the 20-day degradation period, all three GRg3-PNPs exhibited similar degradation profiles and synchronous GRg3 release kinetics. This further confirmed that GRg3 does not significantly interfere with the degradation of PBVHx PNPs or the release profile of the encapsulated drug (Fig. 3**c**). This PNPs-dependent sustained release mechanism can reduce dosing frequency, lower treatment costs, minimize patient discomfort, and potentially reduce the risk of resistance development.

As expected, GRg3 promoted the growth of hBMSCs. Hong *et al*. [27] reported that GRg3 enhanced the proliferation of hBMSCs, inhibited their senescence, and simultaneously promoted their osteogenic differentiation. Our results demonstrate sustained proliferation over 20 days in all groups. However, the viability of cells treated with pPNPs and 1 % GRg3-PNPs consistently remained lower than that of cells treated with 5 % GRg3-PNPs and 10 % GRg3-PNPs. Furthermore, no significant difference existed between the 5 % and 10 % GRg3-PNPs groups (Fig. 5**c,d**), indicating that GRg3 released from PNPs effectively stimulates hBMSC proliferation.

Following 24-hour incubation with PNPs for uptake, hBMSCs underwent osteogenic differentiation assessment for 20 days. Sustained treatment with different GRg3-PNPs revealed that 5 % GRg3-PNPs elicited the strongest osteogenic response (Fig. 6). ALP activity showed no initial differences but became significantly elevated in the 5 % and 10 % GRg3-PNPs groups from day 5 onwards, culminating in levels more than double those of the control groups by day 20. Mineralization (calcium nodule formation) was also highest in the 5 % GRg3-PNPs group on day 20 (Fig. 6**a–d**). This aligns with previous studies indicating that an optimal concentration of GRg3 promotes hBMSC osteogenic differentiation. ALP and mineralization are critical markers of osteogenic commitment; their increased levels signify enhanced osteogenic capacity. Prior studies reported GRg3 stimulation of ALP activity and mineralization in MC3T3-E1 cells and primary osteoblasts [2,3,28].

Furthermore, among the GRg3-loaded PNPs, 5 % GRg3-PNPs most effectively upregulated the four pro-osteogenic markers (*COL-1*, *OCN*, *OPN*, *RUNX2*) and downregulated the two markers associated with osteogenesis inhibition (*MGP*, *OPG*) (Fig. 6). Siddiqi *et al*. [28] found that Rg3 (with a content of 33 %) in red ginseng extract could increase the ALP activity, type I collagen (Col-I) and mRNA expression levels in preosteoblastic MC3T3-E1 cells; they further found that GRg3 could inhibit osteogenesis [4]. Zhang *et al*. [3] demonstrated that GRg3 upregulated *RUNX2*, ALP, *COL-1*, *OCN*, and *OPN* mRNA levels in MC3T3-E1 cells and promoted calcium deposition. These effects are linked to GRg3's direct modulation of multiple signaling pathways governing bone metabolism. For instance, GRg3 directly activates the TGF-β1/Smad pathway [2], regulates the AMPK/mTOR signaling pathway [3], promotes osteogenesis, and inhibits osteoclast differentiation via the RANKL, JNK, and p38 MAPK pathways [4]. Additionally, GRg3 modulates the KPNA2 and NF-κB signaling pathways to influence bone homeostasis and mitigate osteoporosis [5]. These multifaceted actions collectively manifest as the observed upregulation of pro-osteogenic markers and downregulation of markers favoring osteoclastogenesis or inhibiting osteogenesis.

In summary, lower or excessive GRg3 concentrations fail to achieve optimal osteogenic efficacy. This is likely because insufficient GRg3 provides inadequate stimulus, while excessive concentrations may induce cytotoxicity. Consequently, the 5 % GRg3-PNPs, containing a moderate and optimal GRg3 concentration, demonstrated the most potent osteogenic effects.

Conclusions

In this study, we successfully developed a novel nanoparticle system (PNPs) based on the biodegradable natural trimer of PHA (PBVHx) doped with PLGA-PEI, for the efficient delivery of the poorly water-soluble TCM component ginsenoside Rg3 (GRg3). Encapsulating GRg3 within these nanoparticles protects it from degradation, ensures

high local intracellular concentrations, and enables controlled, sustained release. This setup enables the continuous delivery of an appropriate dose of GRg3 to both the intracellular space of stem cells and their extracellular microenvironment, which not only enhances GRg3's regenerative activity and therapeutic efficacy but also ultimately promotes the progression of bone regeneration. It is expected that this development will be vital for the future precise treatment of osteoporosis and bone injuries, with TCM-based strategies applied across various use cases.

List of Abbreviations

ALP, alkaline phosphatase; ANOVA, analysis of variance; ARS, Alizarin red S; 3HB, 3-hydroxybutyrate; BM, Basal Medium; BSA, bovine serum albumin; C6, coumarin 6; CCK-8, cell counting kit-8; CLSM, confocal laser scanning microscope; COL-1, collagen type I; CO_2, Carbon Dioxide; DAPI, 4′,6-diamidino-2-phenylindole; DCM, dichloromethane; DMSO, dimethyl sulfoxide; DL, drug loading; EE, encapsulation efficiency; FBS, fetal bovine serum; GRg3, ginsenoside Rg3; *GAPDH*, glyceraldehyde-3-phosphate dehydrogenase (housekeeping gene); HPLC, high-performance liquid chromatography; hBMSCs, human bone marrow-derived mesenchymal stem cells; JNK, c-Jun N-terminal kinase; KPNA2, karyopherin alpha 2; MAPK, mitogen-activated protein kinase; MGP, matrix Gla protein; mPEG, methoxy poly(ethylene glycol); NF-κB, nuclear factor-kappa b; OCN, osteocalcin; OPG, osteoprotegerin; OPN, osteopontin; PBS, phosphate-buffered saline; PHA, polyhydroxyalkanoate; PBVHx (PHBVHHx), poly(3-hydroxybutyrate-co-3-hydroxyvalerate-co-3-hydroxyhexanoate); PLA, polylactic acid; PLGA, poly(lactic-co-glycolic acid); PLGA-PEI, poly(lactic-co-glycolic acid)-polyethylenimine conjugate; PEI, polyethylenimine; PNPs, PBVHx-based nanoparticles; pPNPs, pure PBVHx nanoparticles (blank control group); PVA, polyvinyl alcohol; RANKL, receptor activator of nuclear factor-kappa b ligand; RUNX2, runt-related transcription factor 2; SEM, scanning electron microscopy; TGF-β1, transforming growth factor-beta 1; TCP, tissue culture plates; TEM, transmission electron microscopy; TCM, traditional Chinese medicine; qRT-PCR, quantitative real-time polymerase chain reaction; 3HHx, 3-hydroxyhexanoate; 3HV, 3-hydroxyvalerate.

Availability of Data and Materials

The data used to support the findings of this study are available from the corresponding authors upon request.

Author Contributions

CJC and FZ contributed to the conceptualization and writing-original draft. DCY, FQS, CYW and JT contributed to the investigation. SWL contributed to the funding acquisition. DXW contributed to the conceptualization, writing-original draft, writing-review & editing, and funding acquisition. All authors agreed to be accountable for all aspects of the work in ensuring that questions related to the accuracy or integrity of any part of the work were appropriately.

Ethics Approval and Consent to Participate

Not applicable.

Acknowledgments

Not applicable.

Funding

This work was supported by grants from the Health Commission of Sichuan Province Medical Science and Technology Program (Grant No. 24WSXT106), the Natural Science Basic Research Plan in Shaanxi Province of China (Grant No. 2024JC-YBMS-706), Collaborative Innovation Project of Zigong Medical Big Data and Artificial Intelligence Research Institute (Grant No. 2023-YGY-1-02), Key Science and Technology Plan Project of Zigong (Grant No. 2024-NKY-01-01), Key Science and Technology Plan of Zigong City (Collaborative Innovation Category of Zigong Integrated Traditional Chinese and Western Medicine Research Institute) (Grant No. 2025ZXY0101), Zigong Key Science and Technology Plan (Collaborative Innovation Project of Zigong Institute of Brain Sciences) in 2022 (No. 2022ZCNK), Zigong Key Science and Technology Plan (Collaborative Innovation Project of Zigong Academy of Medical Sciences) in 2023 (Grant No. 2023YKYXT09); Zigong Public Hospital Reform And High-Quality Development Demonstration Project in 2023 (Grant No. ZG-KY-2023-013).

Conflict of Interest

The authors declare that they have no competing interests.

Supplementary Material

Supplementary material associated with this article can be found, in the online version, at https://??.

References

[1] Wang L, Huang X, Qin J, Qi B, Sun C, Guo X, *et al*. The Role of Traditional Chinese Medicines in the Treatment of Osteoporosis. The American Journal of Chinese Medicine. 2024; 52: 949–986. https://doi.org/10.1142/s0192415x24500393.

[2] Song M, Cui Y, Wang Q, Zhang X, Zhang J, Liu M, *et al*. Ginsenoside Rg3 Alleviates Aluminum Chloride-Induced Bone Impairment in Rats by Activating the TGF-β1/Smad Signaling Pathway. Journal of Agricultural and Food Chemistry. 2021; 69: 12634–12644. https://doi.org/10.1021/acs.jafc.1c04695.

[3] Zhang X, Huang F, Chen X, Wu X, Zhu J. Ginsenoside Rg3 attenuates ovariectomy-induced osteoporosis via AMPK/mTOR signaling pathway. Drug Development Research. 2020; 81: 875–884. https://doi.org/10.1002/ddr.21705.

[4] Siddiqi MH, Siddiqi MZ, Kang S, Noh HY, Ahn S, Simu SY, *et al*. Inhibition of Osteoclast Differentiation by Ginsenoside Rg3 in RAW264.7 Cells via RANKL, JNK and p38 MAPK Pathways Through a Modulation of Cathepsin K: An *In Silico* and *In Vitro* Study. Phytotherapy Research: PTR. 2015; 29: 1286–1294. https://doi.org/10.1002/ptr.5374.

[5] Zhang X, Huang F, Liu J, Zhou Z, Yuan S, Jiang H. Molecular Mechanism of Ginsenoside Rg3 Alleviation in Osteoporosis via Modulation of KPNA2 and the NF-κB Signalling Pathway. Clinical and Experimental Pharmacology & Physiology. 2025; 52: e70019. https://doi.org/10.1111/1440-1681.70019.

[6] Wang J, Yu XF, Zhao JJ, Shi SM, Fu L, Sui DY. Ginsenoside Rg3 attenuated omethoate-induced lung injury in rats. Human & Experimental Toxicology. 2016; 35: 677–684. https://doi.org/10.1177/0960327115597984.

[7] Yang J, Li S, Wang L, Du F, Zhou X, Song Q, *et al*. Ginsenoside Rg3 Attenuates Lipopolysaccharide-Induced Acute Lung Injury via MerTK-Dependent Activation of the PI3K/AKT/mTOR Pathway. Frontiers in Pharmacology. 2018; 9: 850. https://doi.org/10.3389/fphar.2018.00850.

[8] Li L, Ni J, Li M, Chen J, Han L, Zhu Y, *et al*. Ginsenoside Rg3 micelles mitigate doxorubicin-induced cardiotoxicity and enhance its anticancer efficacy. Drug Delivery. 2017; 24: 1617–1630. https://doi.org/10.1080/10717544.2017.1391893.

[9] Jia M, Miao W, Li Y, Guo Y, Zeng J, Gao Y, *et al*. A polymerized probucol nanoformulation with neutrophil extracellular vesicle camouflage for cerebral ischemia-reperfusion injury therapy. The Innovation. 2024; 6: 100761. https://doi.org/10.1016/j.xinn.2024.100761.

[10] Liu J, Zhou Y, Lyu Q, Yao X, Wang W. Targeted protein delivery based on stimuli-triggered nanomedicine. Exploration. 2023; 4: 20230025. https://doi.org/10.1002/exp.20230025.

[11] Xue X, Qu H, Li Y. Stimuli-responsive crosslinked nanomedicine for cancer treatment. Exploration. 2022; 2: 20210134. https://doi.org/10.1002/exp.20210134.

[12] Ding Y, Wang Y, Hu Q. Recent advances in overcoming barriers to cell-based delivery systems for cancer immunotherapy. Exploration. 2022; 2: 20210106. https://doi.org/10.1002/exp.20210106.

[13] Zhang L, Hui J, Ma P, Mi Y, Fan D, Zhu C, *et al*. PEGylation of Ginsenoside Rg3-Entrapped Bovine Serum Albumin Nanoparticles: Preparation, Characterization, and *In Vitro* Biological Studies. Journal of Nanomaterials. 2019; 2019: 3959037. https://doi.org/10.1155/2019/3959037.

[14] Hu J, Wang M, Xiao X, Zhang B, Xie Q, Xu X, *et al*. A novel long-acting azathioprine polyhydroxyalkanoate nanoparticle enhances treatment efficacy for systemic lupus erythematosus with reduced side effects. Nanoscale. 2020; 12: 10799–10808. https://doi.org/10.1039/d0nr01308k.

[15] Wei DX, Cai D, Tan Y, Liu K, Dao JW, Li X, *et al*. Poly(3-hydroxybutyrate-co-3-hydroxyvalerate-co-3-hydroxyhexanoate)-based microspheres as a sustained platform for Huperzine A delivery for alzheimer's disease therapy. International Journal of Biological Macromolecules. 2024; 282: 136582. https://doi.org/10.1016/j.ijbiomac.2024.136582.

[16] Huang XY, Zhou XX, Yang H, Xu T, Dao JW, Bian L, *et al*. Directed osteogenic differentiation of human bone marrow mesenchymal stem cells via sustained release of BMP4 from PBVHx-based nanoparticles. International Journal of Biological Macromolecules. 2024; 265: 130649. https://doi.org/10.1016/j.ijbiomac.2024.130649.

[17] Zhou XX, Huang XY, Zhang M, Ma XY, Yang H, Xu T, *et al*. A BMP6 supply system based on PBVHx nanoparticles promotes the osteogenic differentiation of human stem cells in simulated microgravity. International Journal of Biological Macromolecules. 2025; 319: 145444. https://doi.org/10.1016/j.ijbiomac.2025.145444.

[18] Xu T, Huang XY, Dao JW, Xiao D, Wei DX. Synthetic biology for medical biomaterials. Interdisciplinary Medicine. 2025; 3: e20240087. https://doi.org/10.1002/inmd.20240087.

[19] Ding YW, Zhang ZW, Cui XY, Hu RY, Li Y, Huang SD, *et al*. Zn-Cur nanoparticle-enhanced multifunctional hydrogel platform: Synergistic antibacterial and immunoregulatory effects for infected diabetic wound healing. Chemical Engineering Journal. 2025; 503: 158387. https://doi.org/10.1016/j.cej.2024.158387.

[20] Wei DX, Chen Z. Current situation and challenge of exogenous 3-hydroxybutyrate derived from polyhydroxyalkanoates for elderly health: A review. International Journal of Biological Macromolecules. 2025; 285: 138328. https://doi.org/10.1016/j.ijbiomac.2024.138328.

[21] Ding YW, Li Y, Zhang ZW, Dao JW, Wei DX. Hydrogel forming microneedles loaded with VEGF and Ritlecitinib/polyhydroxyalkanoates nanoparticles for mini-invasive androgenetic alopecia treatment. Bioactive Materials. 2024; 38: 95–108. https://doi.org/10.1016/j.bioactmat.2024.04.020.

[22] Wang H, Zou H, Kong L, Zhang Y, Pang H, Su C, *et al*. Determination of ginsenoside Rg3 in plasma by solid-phase extraction and high-performance liquid chromatography for pharmacokinetic study. Journal of Chromatography. B, Biomedical Sciences and Applications. 1999; 731: 403–409. https://doi.org/10.1016/s0378-4347(99)00238-8.

[23] Ma J, Li N, Wang J, Liu Z, Han Y, Zeng Y. *In vivo* synergistic tumor therapies based on copper sulfide photothermal therapeutic nanoplatforms. Exploration. 2023; 3: 20220161. https://doi.org/10.1002/exp.20220161.

[24] Ji H, Zheng Z, Li S, Xiao X, Tang W, Zhang X, *et al*. Research progress of serum albumin in the field of drug delivery. Interdisciplinary Medicine. 2024; 2: e20240010. https://doi.org/10.1002/inmd.20240010.

[25] Liu J, Zhou Z, Li H, Yang X, Wang Z, Xiao J, *et al*. Current status and challenges in the application of microbial PHA particles. Particuology. 2024; 87: 286–302. https://doi.org/10.1016/j.partic.2023.08.011.

[26] Ren ZW, Wang ZY, Ding YW, Dao JW, Li HR, Ma X, *et al*. Polyhydroxyalkanoates: the natural biopolyester for future medical innovations. Biomaterials Science. 2023; 11: 6013–6034. https://doi.org/10.1039/d3bm01043k.

[27] Hong T, Kim MY, Da Ly D, Park SJ, Eom YW, Park KS, *et al*. Ca^{2+}-activated mitochondrial biogenesis and functions improve stem cell fate in Rg3-treated human mesenchymal stem cells. Stem Cell Research & Therapy. 2020; 11: 467. https://doi.org/10.1186/s13287-020-01974-3.

[28] Siddiqi MZ, Siddiqi MH, Kim YJ, Jin Y, Huq MA, Yang DC. Effect of Fermented Red Ginseng Extract Enriched in Ginsenoside Rg3 on the Differentiation and Mineralization of Preosteoblastic MC3T3-E1 Cells. Journal of Medicinal Food. 2015; 18: 542–548. https://doi.org/10.1089/jmf.2014.3251.

Editor's note: The Scientific Editor responsible for this paper was Kelong Fan.

Received: 17th September 2025; **Accepted**: 31st December 2025; **Published**: 31st March 2026